Plasma Sources Sci. Technol. **16** (2007) 742–749 doi:10.1088/0963-0252/16/4/008

Neutral density profiles in argon helicon plasmas

A M Keesee and E E Scime

Department of Physics, West Virginia University, PO Box 6315, Morgantown, WV 26506, USA

E-mail: amy.keesee@mail.wvu.edu

Received 2 April 2007, in final form 23 July 2007
Published 3 September 2007
Online at stacks.iop.org/PSST/16/742

Abstract
We present an analysis of laser-induced fluorescence and emission spectroscopy profile measurements of the excited states of neutral argon for two different helicon source pressures. Through use of a collisional–radiative model that calculates excited state profiles based on measured electron densities, electron temperatures, and the measured edge neutral pressure, the ground state neutral density profile is determined for each pressure case. The results demonstrate that it is possible to extract the ground state neutral density profile from such measurements and that the degree of ionization at the center ($r = 0$) of a helicon source plasma can vary significantly for a small change in source pressure.

1. Introduction

Helicon source plasmas are used for plasma processing, space simulation, space propulsion, and basic plasma physics studies. While plasma physics studies typically focus on the dynamics of ions and electrons in the plasma, the neutral gas that is present in all plasmas can play a significant role in radiation losses, diffusion, momentum transport, and cooling. To understand the role of neutrals in helicon plasmas, accurate and precise measurements of neutral atom spatial distribution, temperature, density and flow speed are required. In a number of helicon source investigations, the absolute density and spatial distribution of neutral atoms in the source chamber remains an important and unanswered question. For example, although plasma processing applications typically require plasma uniformity, little is understood about the effects of neutral non-uniformity in plasma processing sources [1]. Tynan measured a decrease of ∼20–40% in the radial neutral pressure toward the center of a helicon source, which was in reasonable agreement with a simple 1D diffusion model of neutral transport. Because neutral pressure depends on the product of neutral density and temperature, such measurements cannot distinguish between density and temperature variations. In another investigation, measurements of Alfvén wave damping in helium helicon plasmas by Watts and Hanna were consistent with expectations for wave damping due to ion–neutral collisions [2]. Using both a diffusion model similar to Tynan's and a collisionless transport model, Watts and Hanna determined that at the center of their helicon source, the helium plasma was approximately 3% ionized. In contrast to the Tynan and the Watts and Hanna measurements, Boswell postulated that fully ionized plasmas in the center of helicon discharges were required for pressure balance between the hot plasma in the center and the dense, cold neutrals at the plasma edge [3]. Such hollow neutral density profiles are typical of high temperature laboratory plasmas [4]. However, to the best of our knowledge, the neutral density profile in the low temperature, high-density plasmas typical of helicon sources has never been directly measured.

A few groups have investigated the phenomenon of neutral pumping [5–7] in helicon sources. Gilland *et al* measured axial neutral pressure profiles in a high power helicon source in which they assumed that the neutrals were unheated and that the neutral density was directly proportional to the measured pressure [5]. They found that their axial neutral pressure profile measurements were consistent with the predictions of a one dimensional diffusion model that assumed all neutrals crossing into the center of the discharge through a radial neutral-plasma boundary were ionized and then diffused to the end of the helicon source (with the diffusion being limited by charge-exchange collisions) [5]. Assuming a uniform radial neutral density at each axial location, the reported on-axis neutral and plasma densities indicated that the core plasma was only weakly ionized (<15%).

In a different helicon source experiment, Degeling *et al* hypothesized that neutral pumping was responsible for a

relaxation oscillation between a high-density helicon wave mode and a lower-density, inductively coupled mode [6]. In yet another helicon plasma source, Yoon *et al* incorporated neutral pumping into a global model of plasma density and electron temperature in which they assumed that neutrals were completely depleted from the center of the discharge during the 'high-current phase' of the pulse. Their model yielded current densities that agreed with experimental measurements in their modelled helicon source [7].

In previous work on ion heating and ion flows in the WVU helicon source [8–10], ion–neutral and electron–neutral collisions have been shown to be important mechanisms for wave damping, flow thermalization and ion heating. In fact, edge ion heating in cylindrically symmetric plasmas (which is often observed in our experiments and believed to be evidence of damping of edge-localized slow waves in the helicon source [11, 12]) can also result from the thermalization of ion flow by charge-exchange collisions [13]. Therefore, although poorly understood, the spatial distribution of neutral atoms is important to understanding the physics of helicon sources.

In this work, laser-induced fluorescence (LIF) and passive emission spectroscopy provide non-perturbative measurements of the spatial distribution of neutral atoms in helicon source plasmas. Because both of these optical diagnostic methods probe an excited neutral state, a collisional–radiative (CR) model is needed to relate the measured excited state profile to the bulk, or ground state, neutral spatial distribution. We have previously demonstrated that our method of comparing the CR model with the experimental measurements can yield an accurate ground state neutral density profile [14]. In this work we use the method to compare the ground state neutral profiles for two different helicon source configurations. In section 2 we describe the experimental apparatus used in these experiments. In section 3, we describe the LIF and emission spectroscopy measurement techniques and provide details of the CR model in section 4. Two helicon source configurations are examined in section 5. LIF and spectroscopic measurements for each configuration are reviewed and the spatial distribution of neutrals determined from the measured excited state profiles. A small change in operating pressure is sufficient to significantly change the ionization fraction at the center of the helicon plasma.

2. Experimental apparatus

The Hot hELIcon eXperiment (HELIX) vacuum chamber is a 61 cm long, Pyrex tube 10 cm in diameter connected to a 91 cm long, 15 cm diameter, stainless steel chamber (figure 1). The chamber has one set of four 6″ Conflat™ crossing ports in the center of the chamber and two sets of four $2\frac{3}{4}''$ Conflat™ crossing ports on either side that are used for LIF and spectroscopy diagnostic access. The stainless steel chamber opens into a 2 m diameter space chamber, the large experiment on instabilities and anisotropies (LEIA) [15]. A glass tee is attached to the right end of the Pyrex tube as shown in figure 1. Ten electromagnets produce a steady state axial magnetic field of 0–1400 G in the source. A MKS mass flow controller located in the glass tee is used to introduce gas into the vacuum chamber. Neutral pressures are measured by a Balzers PKR250 full range pressure gauge located in the glass

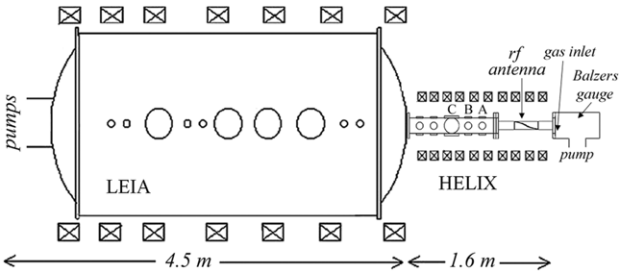

Figure 1. Schematic of HELIX indicating location of (A) Baratron gauge, (B) Langmuir probe and (C) LIF and spectroscopy collection optics.

tee (operating pressures with discharge on) and by a Baratron pressure gauge located 35 cm downstream of the antenna (fill pressures without discharge). Plasmas are created at neutral pressures ranging from 0.1 to 100 mTorr. RF power of up to 2.0 kW over a frequency range of 6–18 MHz is coupled into a 19 cm half wave, right-handed helix antenna to create the steady state plasma. Characteristic electron temperature and density in HELIX are $T_e \approx 4$ eV and $n \approx 1 \times 10^{13}$ cm^{-3} as measured with an rf-compensated Langmuir probe [16] located 50 cm downstream of the antenna.

The 1.5 MHz bandwidth Sacher Lasertechnik SAL-670-15 diode laser used for LIF was mounted in a Littrow external cavity and had a power output of $\leqslant$15 mW and a mode-hop free tuning range of up to 10 GHz ($\approx$0.014 nm) [17]. Wavelength scanning is accomplished by varying the voltage on a piezoelectric controlled grating located within the laser cavity. A National Instruments I/O card provides the voltage ramp to scan the laser frequency, and the linearly polarized laser is mounted on a vibration-isolated platform. The laser light is directed into the plasma with a series of mirrors and beam splitters mounted on the vacuum chamber and the laser table. The optical configuration is described in detail in [17]. A tightly focused set of optics, mounted on a radially scanning assembly located at the crossing ports 65 cm downstream of the antenna, collects the fluorescence light perpendicular to the injected beam and sends the light through a fiber optic cable to a filtered (1 nm wide bandpass) Hamamatsu infrared detector. The detector signal is composed of fluorescence radiation, electron-impact induced radiation and electronic noise. A mechanical chopper operating at a few kHz is used to modulate the laser beam before it enters the vacuum chamber, and a Stanford Research Systems SR830 lock-in amplifier is used to eliminate signals not correlated with the laser modulation. Lock-in amplification is indispensable since the electron-impact induced emission is several orders of magnitude larger than the fluorescence signal. The laser wavelength is tuned to the appropriate transition and monitored for wavelength drift or hops during each scan with a Burleigh WA-1500 wavemeter.

A McPherson™ Model 209 scanning monochromator, consisting of a 1.3 m Czerny-Turner system with a 120 × 140 mm grating, is used for the passive emission spectroscopy diagnostic. The detector is an air-cooled Santa Barbara Instruments Group ST-7XEAI dual autofocusing CCD camera. Light emitted by the plasma is collected by a set of optics mounted on a vertically scanning assembly located at the crossing ports 65 cm downstream of the antenna and is focused

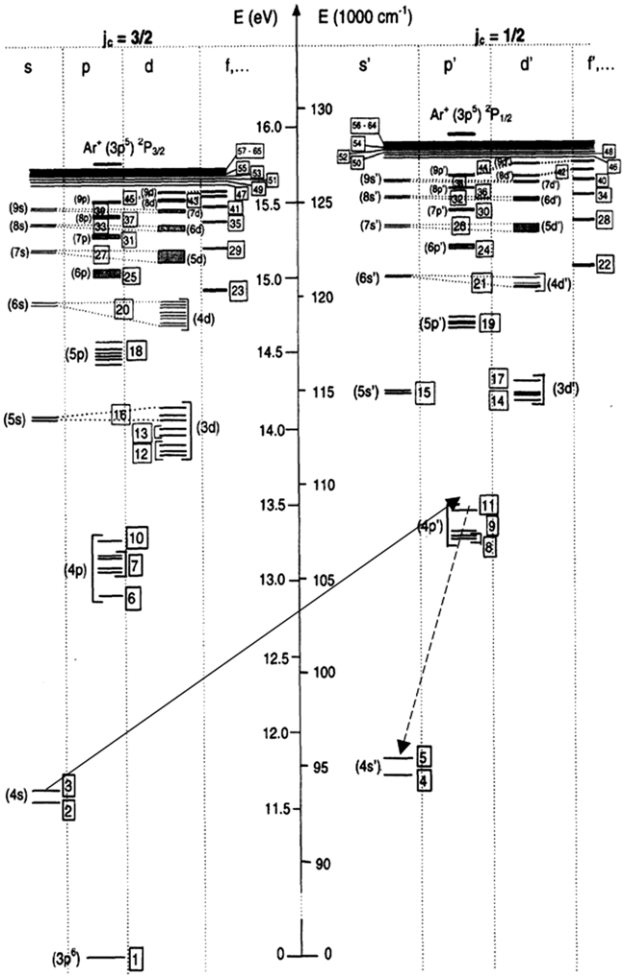

Figure 2. Energy level diagram of argon with identifying numbers for each of the 65 effective levels used in the CR model [29]. The LIF pump (——) and fluorescence (- - - -) lines are indicated.

into a fiber optic cable attached to the entrance slit of the monochromator.

3. Experimental measurements

3.1. Laser-induced fluorescence

Complete details of the argon neutral LIF scheme used with our low power, tunable diode laser have been published previously [18]. Because the initial state of the Ar I LIF sequence is not a metastable state, the scheme requires an electron-impact, collisional excitation transfer from a nearby metastable state to populate the initial state.

Figure 2 shows an energy level diagram of neutral argon. Our three level LIF scheme for Ar I uses laser emission at 667.9125 nm (in vacuum) to pump the $4s[3/2]_1$ state (State 3 in figure 2) to the $4p'[1/2]_0$ state (State 11), which then decays to the $4s'[1/2]_1$ state (State 5) while emitting a photon at 750.5934 nm. This scheme is indicated in figure 2 by a solid arrow for the pump wavelength and a dashed arrow for the fluorescence wavelength. While the $4s[3/2]_1$ state is not a ground or metastable state, we found a sufficient population for LIF due to direct excitation from the ground state and electron-impact excitation transfers from nearby metastable states $4s[3/2]_2$ and $4s'[1/2]_0$ (States 2 and 4, respectively) when operating at high (>10.5 mTorr) pressure.

To obtain reasonable Ar I LIF signal-to-noise, the source was operated at pressures above 10.5 mTorr (operating pressure). Optimal signal–noise was achieved for neutral pressures of approximately 17 mTorr (operating pressure). These relatively high neutral pressures provide the collision rates necessary to populate the initial $4s[3/2]_1$ state from the nearby metastable states. Recently developed, higher power (>100 mW) diode lasers [19] are likely to permit use of this technique over a broader range of plasma conditions. However, the thresholds of neutral density and electron temperature that lead to the population of the target initial state are not yet known.

The LIF signal is directly proportional to the density of the pump state in the collection volume [20]:

$$I \propto \frac{\mathrm{d}\Omega}{4\pi} A_{11,5} \int \mathrm{d}^3x \int \mathrm{d}^3v N_3(x, v) \frac{B_{11,3}}{4\pi} \times \int_0^\infty \mathrm{d}\nu L_{11,3}(\nu, v) W(x, \nu), \quad (1)$$

where $\mathrm{d}\Omega$ is the detector's solid angle, $A_{11,5}$ is the Einstein transition coefficient from State 11 to 5, N_3 is the phase space density of State 3, $B_{11,3}$ is the Einstein absorption coefficient from 3 to 11, $L_{11,3}$ is the absorption line shape of the 3 to 11 transition and W is the laser intensity line shape. The laser linewidth is on the order of a megahertz [21]. For typical helicon source argon plasma parameters, the total absorption lineshape is a convolution of thermal (Doppler) broadening and Zeeman splitting. Because the Doppler width and Zeeman splittings are on the order of a gigahertz, other effects such as the natural linewidth of the line and Stark broadening are ignorable. For the specific Ar I transition used in this work, the Zeeman splitting yields three components [22]. For the π transition, the magnetic orbital quantum number for each level is the same ($\Delta m = 0$). This transition is unshifted from the central wavelength and is linearly polarized along the magnetic field. For the two circularly polarized σ transitions, the magnetic orbital quantum number for each level is different ($\Delta m = \pm 1$). The line shifts for the $\pm\sigma$ transitions in a 1 kG magnetic field are $\Delta\lambda = \pm 2.08 \times 10^{-2}$ Å [23]. Relative intensities of all three Zeeman components obey $I_\pi = 2I_\sigma$.

When the polarization axis of the laser is oriented parallel to the axial magnetic field (perpendicular laser injection), only the π transition is pumped. Because only a single transition is pumped in the Ar I LIF measurements, equation (1) can be integrated over the essentially delta function laser lineshape to yield a LIF intensity that is proportional to the bulk flow shifted Maxwellian distribution of state 3 neutral atoms [24]:

$$I(\nu) = I(\nu_0) \exp\left[\frac{-(\nu - \nu_0 - V_o\nu_0/c)^2}{\alpha_D T_n}\right], \quad (2)$$

where $I(\nu)$ is the measured LIF signal, $I(\nu_0)$ is proportional to State 3 density, $(V_o\nu_0/c)$ is the overall Doppler shift of the distribution due to bulk flow of the neutrals, α_D scales the width of the thermal broadening for neutral argon of mass m_n ($\alpha_D = 2k\nu_0/m_nc^2$), and T_n is the temperature of the neutrals in eV. Because the collection optics are focused along the injected laser beam, the measurement at each horizontal

position of the scanning assembly provides a radially and velocity resolved measurement of the State 3 neutral atom density. The relative State 3 neutral atom density as a function of radial position is obtained by integrating the LIF measurements over laser frequency. A 2D optics scanning assembly is used to obtain profile measurements across an entire plasma cross-section [25].

3.2. Passive emission spectroscopy

The CCD count rate for a transition at a given wavelength, λ, is given by

$$I_{\mathrm{p}}(\lambda) = I_\lambda T_\lambda \Psi_\lambda, \tag{3}$$

where T_λ is the transmission factor of the detection system, and Ψ_λ is the sensitivity of the CCD. I_λ is the line intensity, given by

$$I_\lambda = \frac{h\nu}{4\pi} A_{ki} n_k V \Omega, \tag{4}$$

where $h\nu$ is the energy of the transition ($\nu = c/\lambda$ is the frequency), A_{ki} is the Einstein transition probability for spontaneous emission, n_k is the number of atoms per cubic centimeter in level k, V is the detected plasma volume and Ω is the solid angle subtended by the collection optics [26]. The relative density at each position is obtained by integrating over the measured emission lineshape.

A matrix inversion method [27] is used to determine the radial density profiles from the line-integrated spectroscopic measurements at each vertical position of the collection optics. The inversion assumes cylindrical symmetry, yielding a profile across half the diameter of the plasma. The transitions measured by passive emission spectroscopy were State 11 (see figure 2) to State 3 at a wavelength of 667.9125 nm, State 11 to State 5 at 750.5934 nm and the $4p[1/2]_0$ state (State 10 in figure 2) to State 3 at 751.6720 nm. Since this technique measures the density of the upper state for a transition, the 668 and 751 nm measurements should give the same radial profile when properly normalized.

4. Collisional–radiative model

The CR model used to determine the Ar I excited state populations for a given ground state density and electron distribution function was originally developed by Vlcek [28]; then modified by Bogaerts [29] into a 1D, spatially dependent model for a dc glow discharge. It describes the CR interaction between the 65 lowest energy levels of neutral argon shown in figure 2 [29]. We modified the CR model to match the physical dimensions of HELIX and include only the CR processes relevant to our plasma conditions. The set of coupled equations describing the density $N(n, r)$ of each effective atomic level n at radial position r is given by

$$\frac{\mathrm{d}N(n,r)}{\mathrm{d}t} = R_{\mathrm{gain}}(n,r) - R_{\mathrm{loss}}(n,r) + D\frac{\mathrm{d}^2N(n,r)}{\mathrm{d}r^2}. \tag{5}$$

The processes described by R_{gain} and R_{loss} are

1. Electron-impact excitation and de-excitation between all levels.
2. Thermal argon atom impact excitation and de-excitation between all levels.
3. Radiative decay between all levels.
4. Electron-impact ionization from and three-body recombination to all levels.
5. Thermal argon atom impact ionization from and three-body recombination to all levels.
6. Radiative recombination to all levels.
7. Two- and three-body collisions with thermal ground state atoms for metastable levels. (These collisions are negligible for the other levels because of their low densities.)
8. Metastable–metastable collisions causing ionization of one of the atoms. (These collisions are negligible for the other levels because of their low densities.)

The third term on the right-hand side of equation (5) includes the effects of diffusion for only the metastable states (the short lifetimes of the other excited states make their diffusion negligible). Additional details of the calculations used for each process are described by Vlcek [28] and Bogaerts [29].

The electron energy distribution functions (EEDFs) used in the code are based on electron density and temperature radial profiles measured with an rf-compensated Langmuir probe. As a first step, Maxwellian EEDFs were created based on the measured electron temperatures. An energetic electron beam could then be added to the model Maxwellian distribution to study the effects of a beam on the neutral argon excited levels. The radial profiles of electron density, the EEDFs, and the fill pressure measured at the edge of the chamber are input variables for the code. The parameters describing the ground state profile, as well as the presence and details of an electron beam in the EEDF, were varied until the best match between the measurements and the model was obtained. The percentage of depletion at the center, P, and depletion width, W, are used to parameterize the neutral profile according to

$$\begin{aligned} N(r) &= N_0\left(\left(\frac{2r}{W}\right)^2 + 1\right)(1-P), \qquad -W/2 \leqslant r \leqslant W/2, \\ N(r) &= N_0, \qquad |r| > W/2, \end{aligned} \tag{6}$$

where N_0 is the neutral density found using the ideal gas law based on the input pressure and room temperature at the walls of the chamber. A ground state neutral profile with $P = 0.6$ and $W = 3.0$ is shown in figure 3. Because the Langmuir probe measurements were only obtained for half the diameter of the plasma, cylindrical symmetry is assumed in the CR model.

5. Measurement of neutral profiles

LIF and the emission spectroscopy both provide a measure of the radial density profile of a specific excited atomic state. Thus, each of the measurements must be compared with the appropriate excited state predicted by the CR model for a given ground state neutral density profile to determine the actual ground state neutral density. The LIF measurements can be compared to the model results for State 3, the 668 and 751 nm emission profiles obtained from the matrix inversion can be compared with the model results for State 11, and the 752 nm emission profile can be compared with the model results for State 10 (see figure 2). Neither of the diagnostics is absolutely calibrated, so a peak-to-peak normalization is

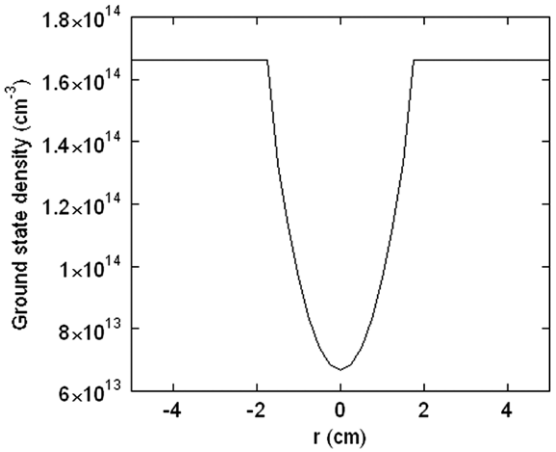

Figure 3. Ground state neutral profile described by equation (6) for $P = 0.6$ and $W = 3.0$.

used for comparison of the measured radial density profile with the profile predicted by the CR model. Because the optical diagnostics average over a finite volume (∼0.5 cm) of plasma and the Langmuir probe measurements have a spatial resolution of less than 2 mm, the CR profiles resulting from the high resolution probe measurements of electron density and temperature have been smoothed with a running window (effective width approximately 0.75 cm).

The density profile of State 3 is the most sensitive to changes in the model input parameters because it is the lowest energy state examined and it is closer in energy to the heavily populated metastable states than States 10 and 11. Thus, any radial structure in the measured plasma parameters, e.g. electron temperature, is most evident in the CR model generated profiles for State 3. Comparison of the LIF measurement of the State 3 density profile with the CR model results for the State 3 density profile was the primary method of determining which neutral density profile best reproduced the measured excited state profiles. Comparison of the emission spectroscopy measurements to the CR predictions for States 10 and 11 were then used as additional checks of the model output. Quantification of the goodness of fit of the CR predictions with the measurements was accomplished with a chi-square test between the two profiles,

$$\chi^2 = \frac{1}{N}\sum_{i=1}^{N}\frac{(L(r_i) - M(r_i))^2}{L(r_i)M(r_i)}, \tag{7}$$

where $L(r_i)$ is the measurement at radial position r_i, $M(r_i)$ is the CR model density value at radial position r_i and N is the number of radial positions measured.

Shown in figure 4 are comparisons of the measured LIF and emission profiles with CR model predictions for a helicon mode plasma operating at 300 W rf power, 750 G magnetic field and 6.0 mTorr fill pressure/18.7 mTorr operating pressure (case A). Note that the emission profiles are strongly peaked in the center of the discharge while the LIF profile is nearly flat. It is the requirement to generate strongly peaked emission profiles with a nearly flat LIF profile that places the strongest constraints on the neutral density profile. Note that the Langmuir probe measurements were only available for one half of the plasma column (figure 5), thus it was not

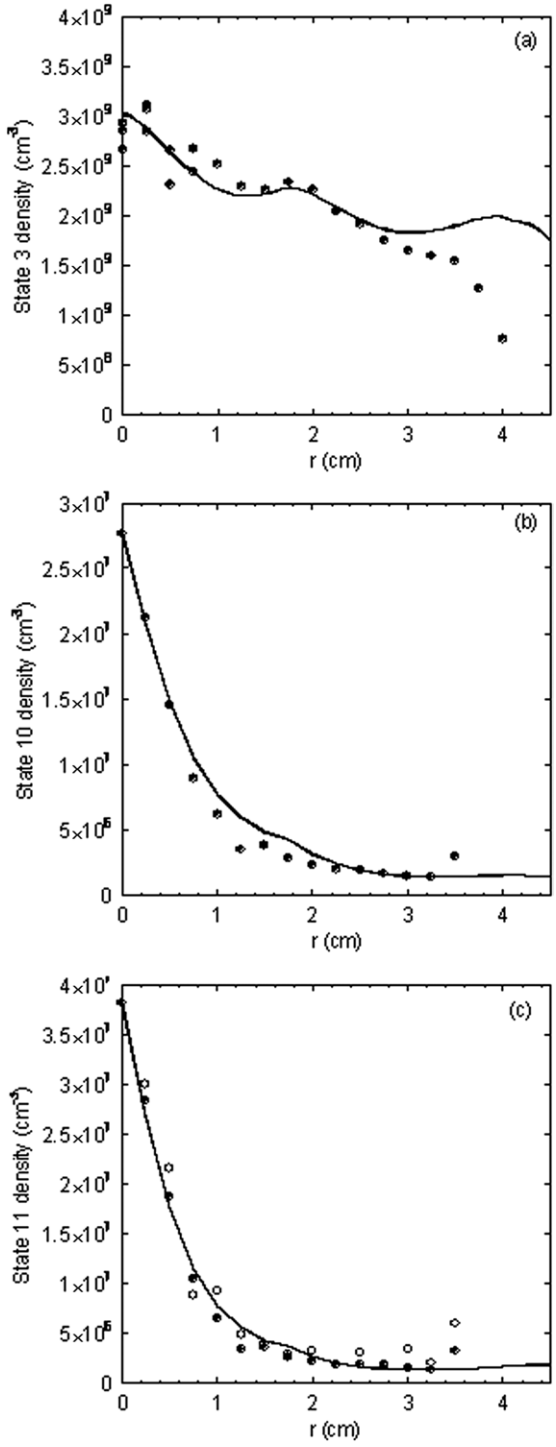

Figure 4. Neutral argon excited state density versus radial position, comparison between experimental data (circles) and CR model output (solid line) for a 3 cm wide depletion of 60%. (*a*) State 3. (*b*) State 10. (*c*) State 11. In (*c*) the nearly identical measured profiles for the 668 nm (open circles) and 751 nm (filled circles) transitions are shown.

possible to run the CR model separately for both halves of the plasma column even though spectroscopic measurements were available across an entire plasma diameter. Over the region where both LIF measurements and Langmuir probe measurements were available, $r > 0$, the CR model and measurements are in good agreement.

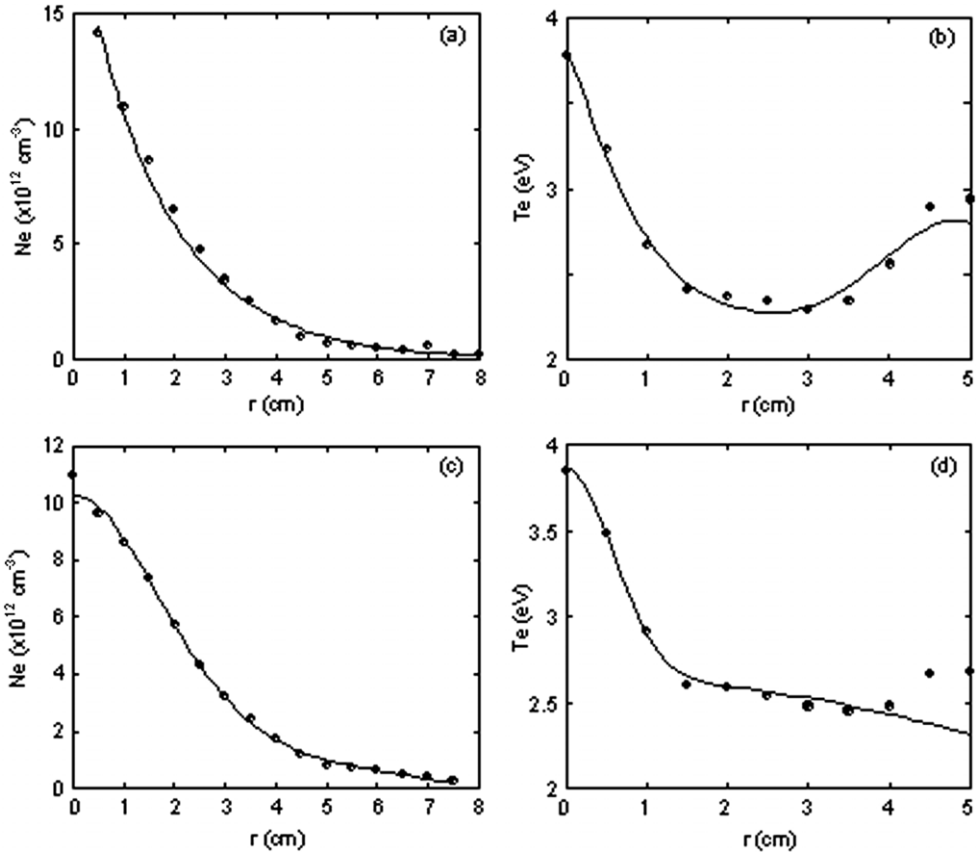

Figure 5. Langmuir probe data with the fits used for CR model inputs for case A (300 W rf power, 750 G magnetic field, 6.0 mTorr fill pressure/18.7 mTorr operating pressure): (*a*) electron density and (*b*) electron temperature. For case B (350 W rf power, 750 G magnetic field, 5.1 mTorr fill pressure/15.1 mTorr operating pressure): (*c*) electron density and (*d*) electron temperature.

The comparisons shown in figure 4 are for a 3 cm wide, 60% neutral density depletion ($P = 0.6$, $W = 3.0$ in equation (6), as shown in figure 3) in the center of the discharge. The chi-square test for State 3 yielded a value of 0.05. When an energetic electron population, an electron beam, was added to the electron distribution function, the model did a poorer job of reproducing the spectroscopic measurements. A number of research groups have reported evidence for energetic electron populations in helicon sources [30–33]. These results suggest that such a population is not required to explain the excited state density profiles in a helicon source. Depletion levels of 55–65% yielded excited state profiles that best reproduced the excited state profile measurements. Different depletion levels (50% or 70%) yielded State 3 profiles that clearly did not match the measured excited state profile.

Note that the LIF intensity (State 3 density) varies by only slightly more than a factor of two across the plasma radius, while the matrix-method inverted emission data (State 10 and State 11 densities) vary by more than an order of magnitude. The key result of this analysis is that the almost flat LIF intensity profile and the inverted emission profile data are both consistent with a hollow ground state neutral profile given the measured electron density and temperature profiles. Such a conclusion can be made only because of the CR model results. Naïve analysis of the raw spectroscopic measurements would indicate a peaked neutral density profile. A flat neutral density profile yields state density profiles that are inconsistent with the LIF and the emission profile measurements. Therefore, this analysis indicates that the neutral depletion at the center is significant for even relatively high-pressure, low-power argon helicon discharges.

Because the CR modeling indicates depletion at the center of the plasma, the ionization fraction at $r = 0$ can be determined more accurately than if only the edge neutral pressure and plasma density at $r = 0$ are known. Using the Langmuir probe measurement of the electron density at $r = 0$ and the neutral density at $r = 0$ as determined by the CR modelling, the ionization fraction, N_e/N_n, of the plasma is 28%. If the edge neutral density were used instead, the ionization fraction would be incorrectly determined to be 11%.

A second, lower pressure, helicon mode plasma (case B), operating at 350 W rf power, 750 G magnetic field, and 5.1 mTorr fill pressure/15.1 mTorr operating pressure, was also investigated. LIF signal was only attainable for 1.5 cm $< r <$ 4.0 cm for these source parameters. Without a full State 3 density profile from LIF measurements, comparison of the CR model and experimental measurements for this source configuration was problematic. If the LIF profile is normalized to that of case A, it can be seen (figure 6) that the increase from the edge to $r = 2$ is about the same in both cases. In figure 7, a similar comparison of the inverted emission spectroscopy data is shown. The inverted emission profiles are more sharply peaked in the center of the plasma for case A than for case B; likely a result of the larger peak plasma density in case A

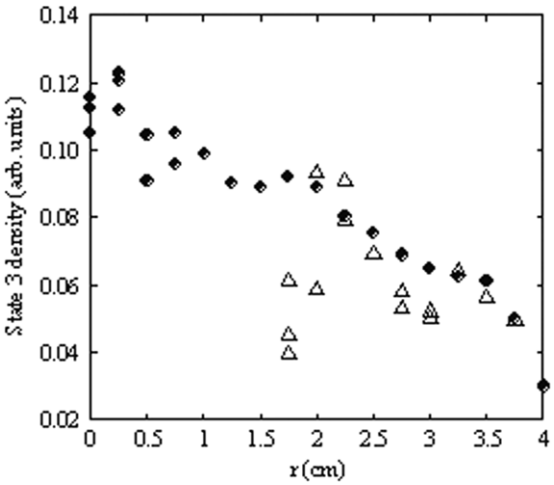

Figure 6. Comparison of State 3 density profiles for cases A (circles) and B (triangles) (as described in figure 5).

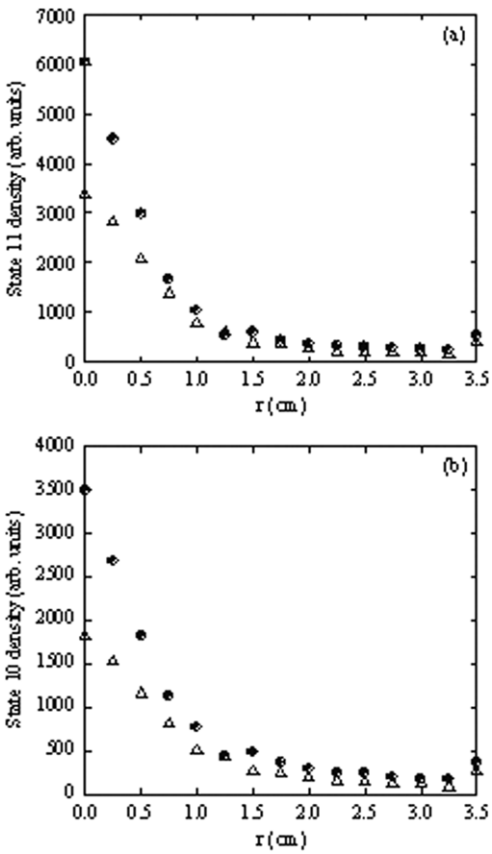

Figure 7. Comparison of (*a*) State 11 and (*b*) State 10 density profiles for cases A (circles) and B (triangles) (as described in figure 5).

(see figure 5). This crude LIF profile comparison, along with the experience gained from many CR model runs, is suggestive of a smaller neutral depletion for the case B helicon source configuration.

Detailed comparison of CR model predictions with the inverted spectroscopy measurements for states 10 and 11 yielded a best match for a ground state depletion of 20% with a width of 3 cm ($P = 0.2$, $W = 3.0$ in equation (6)).

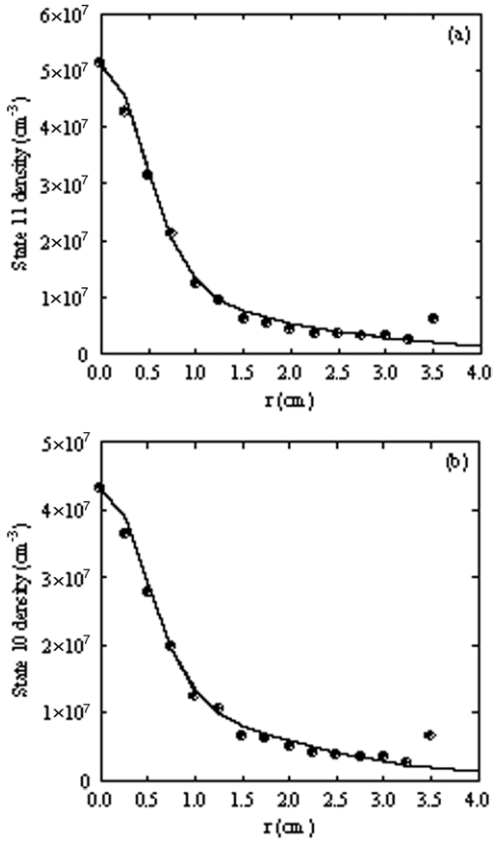

Figure 8. Neutral argon excited state density versus radial position, comparison between experimental data (circles) and CR model output (solid lines) for (*a*) State 11 and (*b*) State 10.

The comparisons are shown in figure 8 and the chi-square test yielded (a) 0.13 and (b) 0.12 for states 10 and 11, respectively. Therefore, consistent with the crude LIF profile analysis, fitting of the CR model to the emission data indicates that the case B helicon plasma has a smaller, ∼20%, neutral depletion at the center of the plasma. Using the CR model results, the ionization fraction at $r = 0$ for this case is 9.8%, quite a bit lower than for case A. Reliance on the edge neutral pressure would yield an incorrect ionization fraction calculation of 7.8%.

6. Conclusions

The combination of spectroscopic measurements and CR model provides a useful tool for non-perturbatively measuring important parameters of ground state species in helicon plasmas. We have successfully measured the ground state argon neutral density profile with a depletion accuracy of approximately ±5% for two cases of helicon mode plasmas with different plasma parameters. For our 6 mTorr helicon mode case, we found that a ground state profile with a 3 cm wide depletion of 60% and a purely Maxwellian EEDF (no electron beam) used in the CR model reproduces the excited state profiles measured using two different optical diagnostics (LIF and emission spectroscopy). For a lower pressure, 5 mTorr helicon mode case, we found that a smaller neutral ground state depletion of 20% reproduces the experimental data; though only emission spectroscopy data were available

for the full radial extent of the source. An important result of this analysis was that contributions to excited state populations by an electron beam yielded predicted excited state profiles that were inconsistent with the measurements.

Calculation of the ionization fraction for the two helicon mode cases indicates that the two source configurations, while employing nearly identical source parameters, yield quite different plasmas. Calculations based on the edge neutral pressure yield ionization fractions of 7.8% and 11% for the 5 mTorr and 6 mTorr helicon mode cases, respectively. However, calculations using the results from the CR modelling yield ionization fractions of 9.8% and 28%, respectively. Only a slight change in plasma parameters leads to a nonlinear change in RF power coupling and therefore a significant difference in the ionization efficiency in the helicon source. The sensitivity to the match conditions was even more evident from measurements in a capacitive mode plasma at 6 mTorr (not presented here). We were unable to find a set of CR model parameters that would yield profiles to match those measured experimentally in the capacitive mode plasma in which most of the RF power is coupled at the edge.

For wave propagation studies, such as Alfvén wave propagation studies recently performed in similar helicon sources [34], the difference in ionization fraction results in substantially different expectations for wave damping and Alfvén wavelengths. Because the Alfvén wavelength depends on the neutral and plasma densities, accurate knowledge of the neutral density leads to better understanding of the propagation and attenuation of Alfvén waves in helicon sources. Therefore, direct measurements of the neutral density at the center of the plasma are required to properly interpret many basic plasma physics experiments performed in helicon source plasmas.

References

[1] Tynan G R 1999 *J. Appl. Phys.* **86** 5356
[2] Watts C and Hanna J 2004 *Phys. Plasmas* **11** 1358
[3] Boswell R W and Porteous K 1987 *Appl. Phys. Lett.* **50** 1130
[4] Hokin S A *et al* 1997 *Nucl. Fusion* **37** 1615
[5] Gilland J, Breun R and Hershkowitz N 1998 *Plasma Sources Sci. Technol.* **7** 416
[6] Degeling A W, Sheridan T E and Boswell R W 1999 *Phys. Plasmas* **6** 1641
[7] Yoon M *et al* 1998 *J. Korean Phys. Soc.* **32** L635
[8] Kline J L, Scime E E, Keiter P A, Balkey M M and Boivin R F 1999 *Phys. Plasmas* **6** 4767
[9] Scime E E, Keiter P A, Zintl M W, Balkey M M, Kline J L and Koepke M E 1998 *Plasma Sources Sci. Technol.* **7** 186
[10] Kline J L, Balkey M, Compton C, Boivin R, Hardin R, Keesee A M, Keiter P, Scime E and Sun X 2003 *Phys. Plasmas* **10** 2127
[11] Kline J, Scime E, Boivin R, Keesee A M, Sun X and Mikhailenko V 2002 *Phys. Rev. Lett.* **88**
[12] Kline J L, Scime E, Boivin R, Keesee A M and Sun X 2002 *Plasma Sources Sci. Technol.* **11** 413
[13] Anderegg F, Stern R A, Skiff F, Hammel B A, Tran M Q, Paris P J and Kohler P 1986 *Phys. Rev. Lett.* **57** 329
[14] Keesee A M and Scime E E 2006 *Rev. Sci. Instrum.* **77** 10F304
[15] Scime E E *et al* 2000 *Phys. Plasmas* **7** 2157
[16] Sudit I D and Chen F F 1994 *Plasma Sources Sci. Technol.* **3** 162
[17] Boivin R F and Scime E E 2003 *Rev. Sci. Instrum.* **74** 4352
[18] Keesee A M, Scime E E and Boivin R F 2004 *Rev. Sci. Instrum.* **75** 4091
[19] http://www.toptica.com/page/news.php
[20] Goeckner M J and Goree J 1989 *J. Vac. Sci. Technol.* A **7** 977
[21] 2000 Sacher Lasertechnik LLC, Instruction Manual, Hannah Arendt Str. 3-7 D35037 Marburg/Lahn Germany
[22] Pauling L and Goudsmit S 1930 *The Structure of Line Spectra* (New York: McGraw-Hill) p 256
[23] Marr G 1968 *Plasma Spectroscopy* (Amsterdam: Elsevier)
[24] Boivin R F 2003 *West Virginia University Plasma Physics Lab Report* PL-050 EPAPS-E-HPAEN-10-003306
[25] Hardin R A, Sun X and Scime E 2004 *Rev. Sci. Instrum.* **75** 4103
[26] Lochte-Holtgreven W 1995 *Plasma Diagnostics* (New York: American Institute of Physics)
[27] Bell R E 1995 *Rev. Sci. Instrum.* **66** 558
[28] Vlcek J 1989 *J. Phys. D: Appl. Phys.* **22** 623
[29] Bogaerts A, Gijbels R and Vlcek J 1998 *J. Appl. Phys.* **84** 121
[30] Chen F F 1991 *Plasma Phys. Control. Fusion* **33** 339
[31] Molvik A W, Ellingboe A R and Rognlien T D 1997 *Phys. Rev. Lett.* **79** 233
[32] Chen R T S and Hershkowitz N 1998 *Phys. Rev. Lett.* **80** 4677
[33] Lieberman M A, Charles C and Boswell R W 2006 *J. Phys. D: Appl. Phys.* **39** 3294
[34] Watts C and Hanna J 2004 *Phys. Plasmas* **11** 1358